Robust Metabolomics Approach For The Evaluation Of Human Embryos From In-Vitro Fertilization.

Cecilia Figoli
CINDEFI-CONICET, CCT La Plata, Facultad de Ciencias Exactas, UNLP
Marcelo Garcea
PREGNA Medicina Reproductiva
Claudio Bisioli
PREGNA Medicina Reproductiva
Valeria Tafintseva
Faculty of Science and Technology, Norwegian University of Life Sciences
Volha Shapaval
Faculty of Science and Technology, Norwegian University of Life Sciences
Mariana Gómez Peña
PREGNA Medicina Reproductiva
Luz Gibbons
Instituto de Efectividad Clínica y Sanitaria (IECS)
Fernando Althabe
Instituto de Efectividad Clínica y Sanitaria (IECS)
Osvaldo Yantorno
CINDEFI-CONICET, CCT La Plata, Facultad de Ciencias Exactas, UNLP
Marcos Horton
PREGNA Medicina Reproductiva
Jürgen Schmitt
Synthon GmbH
Peter Lasch
Robert Koch-Institute, Centre for Biological Threats and Special Pathogens, Proteomics and Spectroscopy (ZBS6) https://orcid.org/0000-0001-6193-3144
Achim Kohler
Norwegian University of Life Sciences
Alejandra Bosch (✉ bosch@quimica.unlp.edu.ar)
CINDEFI-CONICET, CCT La Plata, Facultad de Ciencias Exactas, UNLP https://orcid.org/0000-0002-8243-7577

Article

Keywords: in-vitro fertilization (IVF), Fourier Transform Infrared spectroscopy (FTIR)

Posted Date: February 10th, 2021

DOI: https://doi.org/10.21203/rs.3.rs-153253/v1

ROBUST METABOLOMICS APPROACH FOR THE EVALUATION OF HUMAN EMBRYOS FROM IN-VITRO FERTILIZATION

Cecilia Beatriz Figoli[1], Marcelo Garcea[2], Claudio Bisioli[2], Valeria Tafintseva[3], Volha Shapaval[3], Mariana Gómez Peña[2], Luz Gibbons[4], Fernando Althabe[4], Osvaldo Miguel Yantorno[1], Marcos Horton[2], Jürgen Schmitt[5], Peter Lasch[6], Achim Kohler[3]* & Alejandra Bosch[1,]*

*corresponding authors:

Alejandra Bosch, E-mail: bosch@quimica.unlp.edu.ar

Achim Kohler, E-mail: achim.kohler@nmbu.no

[1]CINDEFI-CONICET, CCT La Plata, Facultad de Ciencias Exactas, UNLP, La Plata, Argentina

[2]PREGNA Medicina Reproductiva, Ciudad Autónoma de Buenos Aires, Argentina

[3]Faculty of Science and Technology, Norwegian University of Life Sciences, 1432 Ås, Norway

[4]IECS, Instituto de Efectividad Clínica y Sanitaria, Ciudad Autónoma de Buenos Aires, Argentina

[5]Synthon GmbH, Schriersheim, Germany

[6]Centre for Biological Threats and Special Pathogens (ZBS) Proteomics and Spectroscopy" Unit, Robert Koch-Institut, Berlin, Germany.

ABSTRACT

The identification of the most competent embryos for transfer to the uterus constitutes the main challenge of *in-vitro* fertilization (IVF). We established a metabolomic-based approach applying Fourier Transform Infrared spectroscopy (FTIR) on 130 samples of 3-days embryo culture supernatants from 26 embryos that implanted and 104 that failed. Examining the internal structure of the data by unsupervised multivariate analysis, it was observed that the supernatants of nonimplanted embryos contained highly heterogeneous spectral features. These features were overlapping with metabolic-implantation fingerprints, thus demonstrating that in establishing embryo-assessment models a one-class modelling involving only the samples with positive-implantation outcomes should be applied. Analysis of variance confirmed that the women´s age (>40 years) undermined the implantation of the embryos exhibiting implantation metabolomics, and also that constituted a condition triggering embryos to express nonimplantation metabolomics. We conclude that IVF-success rates can be significantly improved if FTIR spectroscopy is used as an embryo-selection criterion.

INTRODUCTION

Infertility—a multifactorial disorder that affects around 15% of the reproductive couples worldwide—is a markedly increasing health problem due to the postponement of parenthood[1]. Since the first successful *in-vitro*–fertilization (IVF) birth in 1978, more than eight million children have been born with the help of assisted-reproduction techniques[2,3]. Although IVF is widely used to treat infertile couples, in many instances that approach does not resolve infertility problems because of its low success rate[4]. Several conditions lead to implantation failure, including

reduced endometrial receptivity[5,6], embryonic defects such as genetic abnormalities, the overall clinical status of the mother, faults in the embryo-transfer technique, and/or other multifactorial causes[7,8]. One of the most crucial steps for a successful IVF treatment is definitively the selection of a competent embryo(s) for transfer. The assessment of embryo development and morphology by light microscopy is currently the usual clinically established method for assessing embryo viability[9,10]. This technique constitutes a fast, easy, and affordable evaluation and has been considered as the universally accepted method of choice for embryo selection[9]. Nevertheless, owing to the significant interobserver variability and subjectivity reported in the literature, together with the low capability of morphologic evaluation by light microscopy in predicting the implantation rate of an embryo (*i. .e.*, below 30%), that approach represents an inefficient methodology for embryo selection[11–15]. Alternatively, invasive methods such as the preimplantation genetic testing (PGT) used to determine the genetic profiling of embryos before implantation, involve certain risks, since biopsy might negatively influence further embryo development[16–20]. A noninvasive and rapid evaluation of the embryo-implantation potential before transfer therefore constitutes one of the most crucial challenges in IVF treatments.

In the last decade, metabolomics has emerged as an alternative noninvasive technology to evaluate embryo implantation potential[21]. Human embryos, while developing in the culture media, consume available nutrients and release metabolites, thus modifying culture supernatants. Therefore, a detailed chemical analysis of the spent supernatant of an embryo's culture medium provides information reflecting cellular metabolic activities and the overall developmental status of the embryo. The relationship between the metabolic parameters and embryo viability was reported for the first time in 1980 by Renard and collaborators[22]. A number of proof-of-principle

78 studies related to the chemical composition of embryo's culture supernatants and the
79 subsequent embryo-implantation outcome reported that embryos achieving
80 implantation were different in metabolomic profile from those that failed in
81 implantation[23,24]. Two different approaches were applied in the evaluation of embryo
82 metabolomics: a targeted and a nontargeted metabolic profiling analysis. The former
83 involves multiplexed detection or quantification of predefined metabolites and the
84 establishment of thresholds for those detected[25]. The targeted analysis is based on the
85 hypothesis that embryonic viability is mainly associated with the concentration level
86 of certain products released into the medium, such as those related to energy
87 metabolism (*e. g.*, glucose, pyruvate) and/or the synthesis of extracellular products (*e.*
88 *g.*, lactate and ammonium). In contrast, the nontargeted approach produces
89 metabolomic fingerprints of embryos containing differing multivariate traits that
90 provide insight into the embryo's metabolic state. The extraction of information from
91 these complex metabolic profiles requires a further advanced multivariate data
92 analysis.

93 Several nontargeted technologies like vibrational spectroscopy (near infrared,
94 NIR, and mid-infrared, MIR, plus Raman spectroscopy), nuclear-magnetic resonance
95 (NMR), and matrix-assisted laser desorption/ionization-time-of-flight mass
96 spectrometry (MALDI-TOF) of culture supernatants can provide a complete picture
97 of an embryo’s metabolism and genetic-expression patterns. Therefore, these
98 methodologies have been broadly applied for the evaluation of embryo
99 metabolomics[26]. From 2007 to 2013 studies on metabolomics profiling in spent
100 culture media and the subsequent embryo viability were carried out through the use of
101 different spectroscopy-based technologies[23,27–33]. NIR technologies combined with
102 supervised mathematical models were established to estimate the reproductive

potential of embryos[23,27–33]. Different fertility centers were included in those trials, with the number of recruited patients ranging from 30 to 417. Nevertheless, none of those NIR-based metabolomics models were able to improve clinical-pregnancy rates when compared to the results obtained analyzing embryonic morphology by light microscopy[28,29,31]. In addition, a preliminary MIR-spectroscopy assay demonstrated the great potential of Fourier-transform-–infrared (FTIR) spectroscopy in the screening of the embryonic-implantation potential. Only 7 samples of 26-hour–embryo-culture supernatants from 5 patients were studied, however; and no additional publications with larger cohorts of patients have appeared so far[34]. Finally, Bracewell-Milnes and collaborators (2017), reviewing the potential of the metabolomic technologies as applied to IVF, concluded that the metabolomic profiling of embryo supernatants, as studied up to date, has not evidenced any improvement in the prediction of embryonic viability in clinical practice[26].

FTIR spectroscopy is a nonnvasive analytical physicochemical technique providing information about the total biochemical composition of the analyzed material and has the remarkable advantage of involving a straightforward form of sample preparation and a short spectral-data–acquisition time. FTIR spectroscopy has been successfully used as an analytical tool in a wide range of fields including food, biotechnology, and microbiological and medical diagnostics[35,36,45,37–44]. The potential of FTIR-analysis of blood components (*e. g.*, serum, plasma) and other biofluids (*e. g.*, bile, urine, sputum) for diagnostic purposes has been widely investigated and recognized[46–54]. The great ability of this spectroscopy technology to detect small changes in different types of samples has led to its application in other fields such as the study of extracellular and intracellular metabolites in bacterial[40], fungal[55], and mammalian-cell cultures[38,39]. In particular, glucose, glycerol, and acetic acid were

measured in *Escherichia coli* cultures[40], while glucose and lactate concentrations were evaluated in mammalian-cell lines[38].

From the aforementioned results, we can conclude that the application of vibrational spectroscopy as a diagnostic and prognostic tool has the potential to thoroughly change the assessment of the traditional clinical systems that improve patients healthcare and in so doing enhance the efficiency of the health services[56]. The development of novel technologies for spectral measurement and data analysis increases the possibilities of applying these sophisticated spectroscopic methodologies to routine clinical diagnoses[57].

In view of this strong background, the aim of the present study was to test FTIR spectroscopy combined with multivariate data analysis as a means for a noninvasive assessment of human-embryo metabolomics. For this purpose we characterized 3-day-embryo–culture supernatants by FTIR spectroscopy and evaluated whether changes in the infrared patterns could be associated with the outcome of IVF. Since implantation is a highly complex multifactorial process, we also considered different clinical features with potential impact on implantation rates.

RESULTS

A robust FTIR experimental approach for metabolomic analysis of 3-day-embryo–culture supernatants. In the development of a novel method for the evaluation and selection of embryo-implantation potential based on FTIR vibrational spectroscopy, we established a 3-h protocol for sample preparation and spectral acquisition (Fig. 1). The protocol stated in brief: Supernatants are recovered from individual embryo cultures and centrifuged to remove the culture oil. Then 30 μL are transferred to a 96-multiwell ZnSe optical plate. Next, the samples are dried under

153 moderate vacuum (0.1 bar) for 45 min until transparent films are obtained[52,58].
154 Finally, FTIR transmission-type measurements are carried out in the spectral range
155 650–4000 cm^{-1} at a 6-cm^{-1} spectral resolution.

156 Because FTIR is an extremely sensitive analytical technique, a strict
157 reproducibility analysis was performed to assure the construction of a robust infrared
158 spectral database for further data analysis (Methods). We studied the reproducibility
159 among the measurements obtained for the 96 positions of the ZnSe optical plate using
160 the same batch of fresh culture medium. This analysis demonstrated that the spectral
161 quality was not affected by the desiccation of the samples observed during the lengthy
162 time required for the measurement of 96 samples (Supplementary Fig. 1). A high
163 level of reproducibility was also observed among the samples from each batch and
164 among different batches of G1 Plus culture medium (Supplementary Figs. 2 and 3).
165
166 **FTIR spectral characterization of spent embryo-culture medium.** Fig. 2, Panel a,
167 depicts a representative and exemplary FTIR absorption spectrum of a 3-day-embryo–
168 culture supernatant recovered from a successfully implanted embryo (class IMP in
169 this study), while Fig. 2, Panel b lists the assigned spectral bands and their respective
170 functional groups. The main spectral windows (W1–W5) associated with the
171 molecular building blocks of complex biologic samples[58] could be identified: The
172 spectral region associated preferentially with lipids (W1) between 2800 and 3000 cm^{-1}
173 exhibits bands assigned to the symmetric and antisymmetric C–H stretching modes
174 of methyl groups ($–CH_3$) detected at 2874 and 2969 cm^{-1}, respectively; and the
175 antisymmetric C–H stretching mode for methylene residues ($>CH_2$) at 2933 cm^{-1}. The
176 infrared spectral region associated with protein absorptions (W2) evidenced the
177 typical amide-I and amide-II bands at 1655 and 1545 cm^{-1}, respectively. The mixed

region (W3) between 1200 and 1500 cm^{-1} represents absorptions of stretching and bending vibrations from fatty acids, polysaccharides, nucleic acids, and proteins. A characteristic band is observed around 1400 cm^{-1}, which absorbance may be attributed to the symmetric stretching vibrations of the $–COO^–$ functional groups of amino-acid side chains or free fatty acids. In this region, a typical amide-III band at 1315 cm^{-1} was also observed along with bands of different >P=O asymmetric stretching at around 1230 cm^{-1}. The vibrational modes of the carbohydrate region (W4) between 900 and 1200 cm^{-1} is generally dominated by the symmetric stretching vibration of $PO_2^–$ groups (1090 cm^{-1}) in nucleic acids and a complex sequence of peaks mainly due to the C–O–C and C–O–P stretching vibrations of various oligo- and polysaccharides[58]. That region also contains bands assigned to the C–O stretching vibrations in carboxylic groups—*e. g.*, in lactate at 1041 cm^{-1} and 1120 cm^{-1}[59,60]. Finally, the region between 650 and 900 cm^{-1} (W5) contains weakly expressed bands arising from the aromatic-ring vibrations of phenylalanine, tyrosine, tryptophan, and the various nucleotides. With the exception of only a few peaks (*e. g.*, a band near 720 cm^{-1}, resulting from the $>CH_2$-rocking modes of the fatty-acid chains), valid assignments can hardly be achieved. W5 exhibits a variety of extremely characteristic, features superimposed on an underlying broad spectral contour. Therefore, we refer to this spectral domain as the true fingerprint region[58].

Development of a predictive embryo-implantation model based on the FTIR metabolomic profile of embryo supernatants. The internal structure of the spectral data was studied by the unsupervised multivariate method of principal component analysis (PCA). This analysis aims at transforming the original variables, which here referred to wavenumbers in infrared spectroscopy, into smaller numbers of new

variables or principal components that describe the main variation patterns[61]. The PCA-score plot obtained (Fig. 3, Panel a) revealed that the spectral fingerprints of the supernatants from the implanted embryos (IMP, black squares) were quite similar among themselves and formed a relatively homogeneous cluster in the principal-component space (Supplementary Note 1 and Supplementary Fig. 4). In contrast, the spectra recorded from the supernatants of nonimplanted embryos (class NIMP, green squares) were distributed over a much wider range, thus exhibiting a larger spectral heterogeneity (see Supplementary Note 1 and Supplementary Fig. 4). Of interest to us was that the coordinates of the IMP and NIMP patterns completely overlapped. This observation and the higher heterogeneity level of NIMP fingerprints, suggested the presence of altered metabolic states in the embryos that did not implant. We were tempted to speculate that some of those altered states may be responsible for the nonimplantation. Within this context, we also need to mention, however, that a significant fraction of spectral fingerprints from the nonimplanted embryos (NIMP) proved indistinguishable from the supernatants of the implanted embryos (IMP, *cf.* the overlap in Fig. 3, Panel a). This finding would be in accord with our working hypothesis that certain embryos, though expressing the metabolomic biomarkers for embryo implantation, failed to implant for other reasons. Some of those conditions influencing implantation outcome that are not associated with metabolomics could be *e. g.,* maternal features like overweight, age, and smoking habits, among others.

To test our hypothesis, we employed the method of soft independent modelling of class analogies (SIMCA)[62], a one-class modelling technique that involves only a single class of objects to establish a discrimination model. The model can then be used to classify any new subject as to either belonging to the class or

being outside of the class. This approach is particularly well suited in the example of embryo-supernatant data since embryos with implantation results (IMP) are quite similar among themselves and can be used to establish such a model, whereas the embryos with nonimplantation results (NIMP) are more disparate. Thus, a SIMCA model was established with the spectra of IMP group. The SIMCA model is represented by a class border (see Fig. 3, Panel b, curved line) that separates samples that belong to the class~~)~~ from those falling outside the class. The model then, upon challenge by the NIMP samples, separated that class into two groups. The first contained the so-called "implantation fingerprints" (IF)—*i. e.*, comprising spectra from samples with a metabolic fingerprint similar to IMP (Fig 3, Panel b**,** orange dots). The second class, formed by putative "nonimplantation fingerprints" (NIF), contained spectra from supernatants with altered metabolic states (Fig 3, Panel b, blue dots). We need to note here that the NIMP spectra exclusively—but no IMP samples—are plotted in Fig. 3, Panel b. Therefore, from this plot we can clearly recognize that some NIMP fingerprints belong to the model space characterized by implanted-embryo fingerprints (IF, orange dots) while others fall outside that model space (NIF, blue dots). This situation is also reflected in the logic diagram in Fig. 3, Panel c; which representation illustrates that the class IF was composed of all 26 of the IMP spectra along with 40 of the NIMP spectra having features of the metabolic-implantation fingerprint (the 40 orange dots in Fig. 3, Panel b), all together totalling 66 samples. The NIF class contained the remaining 64 fingerprints from NIMP spectra (blue dots in Fig. 3, Panel b). What was also of interest was that the classification by the SIMCA model provided an almost perfect balance between the IF and NIF classes (*i. e.*, 66 *versus* 64). This observation suggested that, according to our hypothesis, roughly half of the embryos had implantation potential.

An in-depth analysis of the second derivatives of spectra belonging to NIF and IF groups revealed certain spectral differences mainly in the spectral bands associated with amino acids and carbohydrates located within W2 and W4, respectively (Fig. 2). Indeed, a decrease in the intensities of the 1590 and 1530 cm^{-1} peaks were observed in IF in comparison with those of the NIF spectra (Supplementary Fig. 5). This result could be indicative of a difference in the amino-acid turnover between the two groups of embryos. Furthermore, in the spectral regions associated with the lactate-group absorption bands (at 1120 and 1041 cm^{-1}), the IF spectra exhibited more intensive peaks than did the NIF, which difference might represent a higher lactate production due to an increase in glucose uptake in the embryos of the IF group[59,63]. These results also revealed that SIMCA analysis could in fact discriminate between embryos presenting different metabolomic profiles.

To support this hypothesis—and with an aim at identifying potential causes for the embryos with implanting metabolomic fingerprints (IF class) to have failed to implant—different statistical analyses were performed. For this purpose we used the patients´ clinical data registered in the OpenClinica database (*cf.* the methods section). This database contained certain patient parameters that are known to be associated with implantation outcomes such as women's age (between 27 to 42 years classified in three categories, <35, from 35 to 40, and >40), women´s body-mass index ([BMI], divided into 4 classes from normal weight to obesity), and smoking habits (categorized in 5 groups, from nonsmoker to smoker at more than 20 cigarettes per day). Each of these parameters was analyzed independently (one-way analysis of variance [ANOVA]) and in combination (multivariate analysis of variance [MANOVA]). Through this approach, we could confirm that the woman's age was the main factor significantly associated (p <0.05) with the nonimplantation of embryos

278 within the class NIMP classified by SIMCA as the IF class (comprising those having
279 implantation potential; Supplementary Fig. 6, Panel a). Accordingly, upon analyzing
280 the distribution of the mothers' ages, we found that within the IF class the IMP group
281 (those same 26 samples) did not contain women older than 40 years, while the NIMP
282 group (40 samples) included women of all three age-categories (age groups 1, 2 and
283 3; Supplementary Fig. 7, Panel a). Furthermore, we searched if any of the external
284 parameters analyzed here could have triggered the embryos to express either IF or
285 NIF metabolomics. In an ANOVA comparison between the classes IF (26 + 40
286 samples) and NIF (64 samples), we found that the samples predicted as NIF were
287 typical of women of a statistically relevant higher age (Supplementary Fig 6, Panel b).
288 In fact, a comparison of the distribution of the mothers´ ages within IF and NIF
289 revealed that the NIF class contained a higher number of women older than 40 years
290 (Supplementary Fig. 7, Panel b).

291 In view of the morphology grade of the embryos as assessed by the Istanbul-
292 consensus criteria[9], a statistical analysis (chi^2) demonstrated that the morphologic
293 distribution of the embryos (grades 1, 2, and 3) observed within the IF and the NIF
294 classes was also not significantly different (Fig. 3, Panel d, $p = 0.125$). Therefore, a
295 grading system based on the embryo-cleavage rate and morphologic features were
296 found not to be correlated with the different metabolomic patterns obtained by FTIR
297 spectroscopy.

298 At this juncture, we would like to point out some fundamental pragmatic
299 considerations. If FTIR spectroscopy is to be used in a practical arrangement as a
300 method for identifying embryo candidates suitable for implantation, only embryos
301 with the metabolic implantation-fingerprint class IF would be considered, while
302 embryos of class NIF would be disregarded. Under these conditions, the success rate

of implantation in the present study would have equaled ~40%. This value can be obtained by the formula IMP/IF = 26/(26 + 40) = 39.4%. In contrast to such an application, however, the present study employed FTIR spectroscopy only retrospectively after the implantations had been performed. As a consequence, all 64 embryos of the NIF class were transferred because those embryos had met all the morphologic criteria for successful implantation. The success rate in this instance—*i. e.*, without application of the FTIR criteria—was only 20% [IMP/(IMP + NIMP) = 26/(26 + 40 + 64)]. Thus, the success rate achievable with FTIR spectroscopy would have been almost twice as high as the rate of embryo assessment without considering the FTIR criteria. Of course, this retrospective data would need to be carefully reviewed and validated in a larger study. Nevertheless, this example clearly argues that the metabolomic criteria developed in our study have the potential to significantly improve the success rate of embryo implantation.

DISCUSSION

Assisted-reproduction techniques (ART) are globally adopted methods that occupy a central place in reproductive medicine. IVF in particular, enhances the possibility of pregnancy and also enables women to conceive in situations which would not have been possible decades ago[64]. Nevertheless, the success rate of that reproductive treatment is still low (only 30%). Although depending on many different parameters[54], the crucial step of the process is clearly the selection of a fully competent embryo for transfer. Accordingly, obtaining and selecting an embryo with the highest implantation potential is still the key objective within the state of the art in IVF laboratories. Different techniques based on diverse approaches for embryo assessment—*e. g.*, morphokinetics, genetics, proteomics, metabolomics—are

328 constantly being proposed. Among noninvasive metabolomic-based techniques, NIR
329 spectroscopy has represented a widespread analytical technique for carrying out a
330 direct study of embryo supernatants. That approach offers a wide diversity of
331 instrumentation available today, provides the possibility of using portable on-field
332 spectrometers, and further supernatant spectra can be directly measured owing to the
333 limited water interference[65–67]. NIR technology produces very wide bands due to the
334 absorption of few signals from the molecular overtones along with a combination of
335 stretching-bending vibrations of atomic groups such as O–H, C–H, and N–H[67]. The
336 group of Dr. Denny Sakkas at the University of Massachusetts, Boston developed an
337 NIR-based technique combined with supervised mathematical models for embryo
338 selection and applied that procedure to different cohorts of patients. That strategy,
339 however, was unable to further improve pregnancy rates, even when combined with
340 an evaluation of embryo morphology[23,28,29,31–33,68]. In contrast, MIR spectroscopy
341 provides much more information about the biochemical composition of the biologic
342 materials[58]. MIR spectra arise from the stretching and bending vibrations resulting
343 from all bonds that exhibit a transition dipole moment, such as C–H, C=O, C–O, O–
344 H, N–H, C–N, among others. FTIR spectroscopy is hence more sensitive than NIR to
345 the full range of biomolecules present in biologic samples, and even more so when the
346 dried-film technology is applied to guarantee that the strong features of water-
347 absorption bands, which interfere in the spectrum, are avoided[54,56,58,69].

348 In its current state, the NIR technique provides no clinical benefit.
349 Nevertheless we are convinced that the main reason for its low success is not only due
350 to limitations in the spectroscopy technology itself, but also to the data structuring
351 (data classification), and the analytical approaches used for the data analysis. In most
352 of those investigations the available data were first organized in two classes: i)

samples belonging to embryos that implanted or resulted in a live birth and ii) samples belonging to embryos that failed to do either. Then, these two classes served as reference data for training different supervised learning algorithms[54,58]. Supervised data-processing methods such as genetic algorithms, or least-squares regressions use the spectra *a priori* assigned to classes, as teaching information to build models that are later used to predict the outcome of unknown samples. Our great concern at this point is that we demonstrated here that nonimplanted-embryo supernatants (the NIMPs) do not follow any specific pattern. Quite the contrary, these embryos represent a highly heterogeneous group of spectra (Fig. 3, Panel a, Supplementary Note 1, and Supplementary Fig. 4). Moreover, among the NIMP group of samples, a significant number might belong to embryos that could be good candidates on the basis of their metabolomic patterns having biochemical-implantation fingerprints similar to those of the implanted embryos, but failing to implant owing to the other parameters not associated with metabolomics and thus not reflected in spectroscopic methods (*e. g.*, the maternal age for example; Supplementary Figs. 6, Panel a and 7, Panel a). Those samples were therefore falsely grouped in the wrong class from the metabolomics point of view. Consequently, the use of the fingerprints of nonimplanted embryos as one of the references on which to establish an implantation model disregards the reality that implantation is multifactorial.

We need to underscore that in most of the investigations based on molecular methods such as genomics, transcriptomics, or proteomics for embryo-viability–assessment, the data were first preclassified according to implantation outcomes, and supervised models were subsequently formulated with the information contained in both implantation and nonimplantation classes as reference data[23,27–32,34]. Our study presents a completely novel approach for classifying the samples according to their

implantation potential and reveals the underlying reasons for the differences between the implantation and nonimplantation of samples. In the results reported here, we demonstrated that classification models should be established differently from the existing models within the field. We established our classification model using the data of implanted embryos (IMP) in a one-class modelling technique called SIMCA. Utilizing the information of the class with known and homogenous properties (IMP in this study), we were able to predict whether a new sample belonged to the defined class or not. The other class might have a much larger variation that is partially unknown. This approach is highly relevant to the present study since we might encounter an embryo with a different metabolic fingerprint that was not accounted for in the existing sample set. Upon applying SIMCA modeling, the IMP and NIMP groups become redefined into two new classes according to the implantation fingerprint (IF and NIF; Fig. 3, panels b and c).

With respect to our SIMCA model, many embryos presenting metabolomic implantation-fingerprints did not implant (40 NIMP embryos included in the IF group, Fig. 3, Panel c). Thus, those embryos did not implant even though they had an implantation potential according to our model. The successful implantation of an embryo relies on intricate and multiple contributions—not only from eggs and sperm, which determine the quality of resulting embryos—but also from the endometrium, ovarian-stimulation regimes, laboratory conditions, and many external parameters[70]. We indeed were able to demonstrate that those NIMP embryos with metabolomic implantation fingerprinting IF (40 samples in Fig. 3, Panel c) did not implant because of the multifactorial nature of the outcome in pregnancy. An ANOVA analysis of the patients' data recovered in this study (maternal age, BMI, smoking habits), revealed

that maternal age represented at least one of those causes for nonimplantation of these NIMP-IF embryos.

Another question that we could address was if external parameters could negatively influence embryos to express either an implantation metabolomics or a nonimplantation metabolomics. Again, we found that the maternal-age distribution was at least one of the features that differentiated embryos IF from NIF (Supplementary Fig. 6, Panel b and Fig. 7, Panel b). That the strongest influence related to a woman's chance to become pregnant is her age is well known[71–77]; with advanced age causing a reduction in the ovarian follicular pool, perturbations in ovulation, and an increase in meiotic errors within the oocyte[64,78]. This is one among several different clinical predispositions that could induce an embryo to express an implantation or nonimplantion metabolomic fingerprint. To the best of our knowledge, the present study is the first to combine embryo-metabolomic data with patient clinical features.

Different strategies can be described for the process of selecting the embryo with the highest probability of implantation within an embryo cohort. The first represents the development of models that identify embryo biomarkers associated with embryo "quality". In this regard, we can apply different approaches—namely, those based on embryonic morphology (microscopic morphologic analysis, time-lapse imaging techniques), on the quality of the embryo's genetic material (noninvasive PGT), or on embryo metabolomics (NIR, FTIR, Raman, proteomics methods). Then, if a large cohort of patients were available, by combining more than one of these different approaches to assess embryonic viability, a further improvement in developing robust multifactorial implantation models for selecting of the best embryo for transfer would also be possible. Nevertheless, even then, we still could not ensure

427 that such embryos with the best “score” would implant. We have demonstrated here
428 that suitable candidates from the metabolomic point of view, may fail in their
429 implantation owing to other parameters, of equal consequence, associated with
430 patients´ life-style, habits, and/or external characteristics such as smoking habits,
431 BMI, age, stress—in addition to the embryo-transfer quality—just to mention a few.
432 Consequently, a margin of uncertainty involving the patients´ profile and external
433 conditions will always exists, which elements are often difficult to include in a model.
434 Therefore, our present experience would dictate that, to enhance the efficiency of IVF
435 procedures, efforts should focus particularly on two aspects i) combining different
436 approaches for embryo assessment (morphokinetics, genetics, proteomics,
437 metabolomics), and ii) improving data treatment. The combination of different
438 embryo-assessment methods could enable the evaluation of an embryo's complete
439 status with respect to implantation outcome. This multimodal approach could then
440 improve the possibilities for embryologists to select embryos with the highest
441 implantation potential.

442 In this work, we have demonstrated for the first time the potential of FTIR
443 spectroscopy combined with multivariate analysis for gaining insights into
444 fundamental aspects associated with embryo metabolomics and for improving
445 implantation outcomes. In a retrospective analysis examining the combined results of
446 FTIR and SIMCA, we observed that within the NIMP group more than 50% (64 out
447 of 104 embryos) presented an NIF pattern (Fig. 3, Panel c). Thus, these NIMP-NIF
448 embryos would not have been transferred to mothers if they had first been analyzed
449 by the approach employing both FTIR and SIMCA. We need, however, to remark that
450 the criterion for selecting the embryos for transfer was based largely on their
451 morphologic appearance (86% of these embryos presented the highest morphology

grade according to the Istanbul consensus). Therefore, our results indicate that a reconstruction of the data including SIMCA in the IF and NIF will certainly be helpful as a practical adjunct since this additional information would decrease the failure rates and significantly improve the overall IVF outcome. Nonetheless, these results definitely have to be verified experimentally in a follow-up study.

In conclusion, this work has established the basis for how embryo data should be analyzed in order to develop new models for embryo selection in IVF treatments. This research therefore constitutes a significant contribution in the area of assisted fertilization, by offering a novel approach for embryo assessment in IVF treatments and revealing the cause of the failure to establish a reliable metabolomics-based model to predict embryo-implantation outcome.

MATERIALS AND METHODS

Ethical approval. Participants were recruited and provided written consent according to Section IRB00001745-IORG 0001315 of the protocols approved by a national ethics committee for medical education and clinical research [Centro de Educación Médica e Investigaciones Clínicas Norberto Quirno (CEMIC), Argentina].

Patients. The patients participating in the study were recruited from the fertility center "PREGNA-Medicina Reproductiva", Buenos Aires, Argentina, during the period from October 2012 through December 2015.

All women below 42 years old treated at PREGNA and undergoing IVF treatments were considered for participation in the study, but patients with more than two previous IVF attempts were excluded. The diagnosis of the cause of female or male infertility, the protocol applied for ovarian-stimulation, and whether the

conventional IVF or an intracytoplasmic sperm injection was employed were not considered as exclusion criteria. The stimulation protocols consisted of the application of gonadotropins and the gonadotrophin-releasing–hormone antagonist in combination with recombinant and/or highly purified urinary gonadotropins.

Embryo culture. Upon oocyte retrieval, cumulus-oocyte complexes were placed in four-well plates containing 500 µL of G-IVF Plus medium covered with mineral oil (OVOIL-Culture Oil) to avoid evaporation (all the culture media used in this study were from Vitrolife, Göteborg, Sweden). In parallel, semen samples were processed through discontinuous 90–50% density gradients (Spermgrad) and double washed in sperm preparation medium. The sperm suspension was adjusted to 200.000 motile sperm/mL in that medium and kept at room temperature (20–23 ºC) until insemination. For conventional IVF, insemination was carried out 4 h after oocyte retrieval in the G-IVF Plus culture medium. For intracytoplasmic sperm injection, cumulus cells and the corona radiata of oocytes were removed by a brief exposure to 80 IU/mL of hyaluronidase (Hyase-10X) 3–4 h after collection. This fertilization procedure was performed according to the standard protocol[79,80].

After 18–20 h postinsemination, the fertilization was checked and two pronuclei-stage embryos were cultured individually in 40-µL droplets of overnight-equilibrated G-1 Plus medium covered with culture oil in an IVF Tri-gas Incubator Model G185 (K-Systems, Birkerød, Denmark). For each cohort of embryos a drop of G1 Plus medium was incubated under the same conditions as a control.

Embryos incubated for 3 days were individually observed by optical microscopy for morphological grading according to the Istanbul-consensus criteria (European Society of Human Reproduction and Embryology and the Alpha Scientists'

Special-Interest Group)[9]. The embryos were classified as grade 1 (good quality), grade 2 (fair quality), grade 3 (poor quality) and grade 4 (arrested or undeveloped).

The highest-quality embryos from each cohort (one or two) were selected to be transferred. All the single embryos were retrieved from their supernatants. In all instances, only fresh embryos were transferred as described elsewhere after placing them in G-2 Plus culture medium[81]. Spent supernatants, drops of control culture media, samples of different batches of the G-1 Plus culture medium, and samples of the culture oil used were registered and stored under liquid nitrogen for further FTIR spectral analysis.

FTIR spectroscopic analysis. The dried-film FTIR technology[54,56,58,69] was applied to analyze the 3-day-embryo–culture supernatants. For this purpose, a protocol for sample preparation was optimized. Cryopreserved supernatants were thawed at room temperature (25 °C) and centrifuged for 5 min at 1690 x *g* to separate possible remnants of the culture oil in the samples. Different volumes of supernatants (15, 20, and 30 µL) were then pipetted onto each well of a ZnSe 96-well microtiter plate. The samples were dried under moderate vacuum (0.1 bar) or until transparent films were formed[52,58]. FTIR absorption spectra were measured in a Vertex 70 FTIR spectrometer coupled to the high-throughput HTS-XT automatic module under dried-air circulation (Bruker Optics GmbH, Ettlingen, Germany). The spectra were recorded in the transmission mode within the spectral range between 650 and 4000 cm^{-1} with a 6 cm^{-1} spectral resolution by taking 64 scans that were subsequently averaged. Before each sample measurement, background spectra of the ZnSe substrate were collected in order to account for variation in water vapor and CO_2, with OPUS spectroscopy software (version 7.0; Bruker Optics GmbH, Ettlingen, Germany) being used for

527 automatic spectral acquisition. The FTIR spectra of both, the different batches of the
528 culture medium and of the culture oil, used for the different reproducibility studies
529 here performed, were likewise measured according to the procedure described above.
530
531 **Data analysis.** The data-analysis flow sheet applied in this study was specifically
532 developed for the optimized processing of embryo-supernatant FTIR spectra and
533 comprised the following routines: 1) data preprocessing, 2) construction of the FTIR
534 database, 3) hierarchical-cluster analysis (HCA), 4) principal-component analysis
535 (PCA), 5) soft independent modelling of class analogy (SIMCA), and 6) statistical
536 analysis (Fig. 4).
537 Data pretreatment. In order to increase the quality of the FTIR spectral features, to
538 reduce interference from noise, and to avoid interfering signals from water vapor and
539 culture oil that could mask the spectral biomarkers specifically associated with
540 implantation; a spectral preprocessing was applied[82]. As a first step, all raw spectra
541 were subjected to a quality test of our own design through the use of OPUS-
542 spectroscopy software 7.0 (Bruker Optics, Ettlingen, Germany). This test involved
543 checking the following parameters: (i) absorbance in the amide I region (1600–1700
544 cm^{-1}) with acceptable values being between 0.125 and 1.20 absorbance units, (ii) the
545 signal-to-noise ratio (calculated from the first derivatives of the spectra between 2000
546 and 2100 cm^{-1}) with admissible values being lower than 1.5 x 10^{-4} and, (iii) water-
547 vapor content (determined from the first derivatives of the absorbance values between
548 1837 and 1847 cm^{-1}) with acceptable values being lower than 3 x 10^{-4} [52,58]. Because
549 of small quantities of culture oil that were always left in the supernatants after the
550 centrifugation, which could further interfere with FTIR spectral signals; an additional
551 parameter in the quality test, the so-called "λ", was defined. Parameter λ indicates the

552 level of contamination of the supernatant with the culture oil in the infrared-
553 absorbance spectra as follows: the rate of the intensity of the peak at 2933 cm^{-1}
554 assigned as C–H stretching of $>CH_2$ groups (lipids)—used as a marker band of oil
555 content (I_{2933})—and the intensity of the peak at 1655 cm^{-1} assigned to amide I—used
556 as an internal standard of the total biomass (I_{1655}, where $\lambda = I_{2933}/I_{1655}$; Supplementary
557 Fig. 8). Only spectra with $\lambda \leq 0.33$ were included in the FTIR database.

558 For spectra that passed the quality test two different types of spectral
559 preprocessing were developed: one for technical-reproducibility analysis which was
560 applied among i) the different wells of the ZnSe optical plate, ii) the samples of the
561 different culture medium batches, and iii) the samples recovered within each culture
562 medium batch. Another preprocessing was applied to the spectra of supernatant
563 samples before the PCA and SIMCA analyses. In the first, the so-called preprocessing
564 *A*, spectra were preprocessed by calculating the second derivative (Savitzky-Golay, 17
565 windows size) in the regions 2800–3000, 1500–1800, 1250–1500, and 900–1200 cm^{-1}
566 ; in the second, the so-called preprocessing *B*, data were preprocessed by taking the
567 second derivatives (Savitzky-Golay, 3rd-degree polynomial, 17 windows size) in the
568 regions 1500–1800, and 730–1280 cm^{-1}, with extended multiplicative signal
569 correction (EMSC) applying linear term[61].

570 These spectral-preprocessing approaches enabled an increase in the resolution
571 and a more facile interpretation of the spectra along with the detection and removal of
572 outliers. Higher robustness and improved accuracy in subsequent classifications and
573 quantitative analyses are therefore achieved[52,58,82,83].

574 Construction of the FTIR database. To facilitate the subsequent data analysis, an FTIR
575 spectral library was developed containing normalized derivative spectra of 1) spent
576 supernatants, 2) samples from different batches of the culture medium G-1 Plus, and

3) samples from the culture oil used during the study. All the spectra and the corresponding normalized derivatives were classified in two groups (Fig. 5). *Group A* comprised spectra of control samples: culture media, different batches of the culture medium G-1 Plus, and the culture oil. *Group B* consisted of spectra of the supernatants of the embryos that were transferred to the patients, with the IMP group constituting the spectra of supernatants from embryos that implanted (100% implantation), and the NIMP group the spectra of supernatants from nonimplanting embryo (0% implantation).

The supernatant spectra of the group IMP pertained to embryos whose morphologies were 30.8% grade 1 and 69.2% grade 2, where embryos of grade 3 were not found, whereas the supernatants of the NIMP group contained 33.7%, 50.0%, and 16.4% of embryos with morphologies of grades 1, 2, and 3, respectively.

Hierarchical cluster analysis (HCA). This unsupervised-analysis technique was used for checking the reproducibility of the measurements and to detect outliers in the data sets[46]. As previously reported[52,84,85], the spectral variances in the data were determined as the average ± 2 standard deviations of the so-called spectral distance (D). This parameter corresponds to a dissimilarity measurement equal to $(1 - r) \times 1000$, with r being Pearson's product-moment–correlation coefficient. For estimating the reproducibility of measurements among samples within the same batch and among different batches of G1 Plus culture medium, the spectral distances were calculated by using the prepossessing procedure *A* (*cf.* Section Data pretreatment; Supplementary Figs. 1–3). The fusion values in dendrograms were obtained by using the average linkage (OPUS versions 7.0 Bruker Optics GmbH, Ettlingen, Germany).

Principal Component Analyis (PCA). To study the underlying pattern in the data, a PCA analysis of the FTIR metabolomic fingerprints of the 3-day-embryo supernatants

602 was performed. For this purpose the data were analyzed by applying the
603 prepossessing procedure *B* (*cf.* Section Data pretreatment). This analysis was carried
604 out by using Matlab-based in-house algorithms (Matlab R2019a, The MathWorks
605 Inc., Natick, MA).
606 Soft independent modelling of class analogy (SIMCA). For separating the embryo
607 supernatant with implantation-fingerprint spectra from those with nonimplantation
608 spectral fingerprints, the SIMCA[62] pattern-recognition method was employed. The
609 model was established by using class-IMP data only. The spectra were preprocessed
610 by the procedure *B* (*cf.* Section Data pretreatment). To perform SIMCA analysis the
611 Matlab GUI tool DD-SIMCA was used[86]. SIMCA relies on PCA and enables the
612 creation of a border—a hyperplane—around a class of objects (class IMP in this
613 instance) with the type of confidence interval that can be constructed by using
614 different significance levels. The number of components for the PCA model was fixed
615 to 3 and corresponds to a ~90% explained variance. The significance level was set at
616 0.01. After the model was established, preprocessed spectra from the class NIMP
617 (nonimplanted embryo spectra) were used to discriminate embryos that fell within the
618 model's borders (*i. e.*, with an IF-class implantation fingerprint in this instance) from
619 those outside that model exhibiting no implantation fingerprints (the NIF class).
620 Statistical analysis. An ANOVA was performed on the maternal metadata, with the IF
621 class being considered separately, and on the IF *versus* the NIF class obtained by
622 SIMCA modelling. Different parameters such as the maternal age, body-mass index
623 (BMI), and smoking habits were analyzed as a single parameter both separately by
624 ANOVA and all together by the MANOVA.
625 Chi^2 analysis was performed to evaluate the embryo distribution within the IF
626 and NIF classes.

627

628 **Construction of a database platform for research-data management—**
629 **"OpenClinica".** This research was performed under strict international biosafety
630 regulations, applying the "Best Practices for Research Data Management". For this
631 purpose, we used an open-source software OpenClinica, based on electronic forms
632 and protocols for storage, classification, analysis, and data visualization[87]. For the
633 construction of this database, information was registered such as the patients' personal
634 details, hormonal treatments, embryo morphology, pregnancy outcome, and results
635 from the quality tests of the acquired spectra. This platform is currently operating
636 effectively on the web site https://www.openclinica.com/. The data registered at the
637 OpenClinica database like the mother's age, BMI, and smoking habits were converted
638 from numerical variables into qualitative ones.

639 The mother's age was categorized in 3 groups: Group 1, women older than 27
640 and younger than 35 years; Group 2, women between 35 and 40 years; and Group 3,
641 women older than 40 years.

642 The BMI was calculated in each individual by using the patient's height and
643 weight information in the formula (weight in kg)/(height in m)^2 and then classified
644 into 4 groups. Those patients with BMI values between 18.5 to 25.0 (normal weight),
645 were included in Group 1, BMI values below 18.5 (underweight) were placed in
646 Group 2, BMI values between 25.0 to 30.0 (overweight) corresponded to Group 3,
647 and those with BMI values over 30.0 (obesity) were categorized in Group 4.

648 The information related to smoking habit provided by the mothers was divided
649 into 5 categories: Group zero (0), women that never smoked; Group 1, ex-smokers
650 that used to consume fewer than 10 cigarettes per day; Group 2, ex-smokers that used
651 to smoke more than 10 cigarettes per day; Group 3, woman smoking at the time of the

IVF treatment at least 9 cigarettes per day; Group 4, active smokers of 10 to 19 cigarettes per day; and Group 5, smokers of 20 or more cigarettes per day.

REFERENCES

1. Mascarenhas, M. N., Flaxman, S. R., Boerma, T., Vanderpoel, S. & Stevens, G. A. National, Regional, and Global Trends in Infertility Prevalence Since 1990: A Systematic Analysis of 277 Health Surveys. *PLoS Med.* (2012). doi:10.1371/journal.pmed.1001356
2. De Geyter, C. Assisted reproductive technology: Impact on society and need for surveillance. *Best Pract. Res. Clin. Endocrinol. Metab.* **33**, 3–8 (2019).
3. Adamson, G. *et al.* International Committee for Monitoring Assisted Reproductive Technology: world report on assisted reproductive technology, 2016. (2020).
4. Adamson, G. D. *et al.* International Committee for Monitoring Assisted Reproductive Technology: world report on assisted reproductive technology, 2011. *Fertil. Steril.* **110**, 1067–1080 (2018).
5. Kasius, A. *et al.* Endometrial thickness and pregnancy rates after IVF: A systematic review and meta-analysis. *Hum. Reprod. Update* **20**, 530–541 (2014).
6. Lebovitz, O. & Orvieto, R. Treating patients with 'thin' endometrium-an ongoing challenge. *Gynecol. Endocrinol.* **30**, 409–414 (2014).
7. Margalioth, E. J., Ben-Chetrit, A., Gal, M. & Eldar-Geva, T. Investigation and treatment of repeated implantation failure following IVF-ET. *Hum. Reprod.* **21**, 3036–3043 (2006).
8. Roberts, S. A., Hann, M. & Brison, D. R. Factors affecting embryo viability and uterine receptivity: insights from an analysis of the UK registry data. *Reprod. Biomed. Online* **32**, 197–206 (2016).
9. Alpha and ESHRE. The Istanbul consensus workshop on embryo assessment: proceedings of an expert meeting † Alpha Scientists in Reproductive Medicine and ESHRE Special Interest Group of Embryology. *Hum. Fertil.* **26**, 1270–1283 (2011).
10. Nel-Themaat, L. & Nagy, Z. P. A review of the promises and pitfalls of oocyte and embryo metabolomics. *Placenta* **32**, S257–S263 (2011).
11. Botros, L., Sakkas, D. & Seli, E. Metabolomics and its application for non-invasive embryo assessment in IVF. *Mol. Hum. Reprod.* **14**, 679–690 (2008).
12. Katz-Jaffe, M. G. & McReynolds, S. Embryology in the era of proteomics. in *Fertility and Sterility* **99**, 1073–1077 (2013).
13. Andersen, A. N. *et al.* Assisted reproductive technology in Europe, 2004: results generated from European registers by ESHRE. *Hum. Reprod.* **23**, 756–771 (2008).
14. Paternot, G. *et al.* Intra- and interobserver analysis in the morphological assessment of early stage embryos during an IVF procedure: A multicentre study. *Reprod. Biol. Endocrinol.* **9**, 1–5 (2011).
15. Matson, P. L. Internal quality control and external quality assurance in the IVF laboratory. *Hum. Reprod.* **13**, 156–165 (1998).
16. Harper, J. *et al.* Adjuncts in the IVF laboratory: Where is the evidence for 'add-

on' interventions? *Hum. Reprod.* **32**, 485–491 (2017).
17. Lu, M. man *et al.* Trophectoderm biopsy reduces the level of serum β-human chorionic gonadotropin in early pregnancy. *Fertil. Steril.* (2020). doi:10.1016/j.fertnstert.2020.05.015
18. Gordon, C. E. & Racowsky, C. Trophectoderm biopsy—perhaps not such a benign intervention. *Fertil. Steril.* 1–2 (2020). doi:10.1016/j.fertnstert.2020.06.027
19. Penzias, A. *et al.* The use of preimplantation genetic testing for aneuploidy (PGT-A): a committee opinion. *Fertil. Steril.* **109**, 429–436 (2018).
20. Rosenwaks, Z. *et al.* The pros and cons of preimplantation genetic testing for aneuploidy: clinical and laboratory perspectives. *Fertil. Steril.* **110**, 353–361 (2018).
21. Leese, H. J. Metabolism of the preimplantation embryo: 40 years on. *Reproduction* **143**, 417–427 (2012).
22. Renard, J. P., Philippon, A. & Menezo, Y. In-vitro uptake of glucose by bovine blastocysts. *Reproduction* **58**, 161–164 (1980).
23. Seli, E. *et al.* Noninvasive metabolomic profiling of embryo culture media using Raman and near-infrared spectroscopy correlates with reproductive potential of embryos in women undergoing in vitro fertilization. *Fertil. Steril.* **88**, 1350–1357 (2007).
24. Sakkas, D. Embryo selection using metabolomics. *Methods Mol. Biol.* **1154**, 533–540 (2014).
25. Ballin, N. Z. & Laursen, K. H. To target or not to target? Definitions and nomenclature for targeted versus non-targeted analytical food authentication. *Trends Food Sci. Technol.* **86**, 537–543 (2019).
26. Bracewell-Milnes, T. *et al.* Metabolomics as a tool to identify biomarkers to predict and improve outcomes in reproductive medicine: A systematic review. *Hum. Reprod. Update* **23**, 723–736 (2017).
27. Ahlström, A. *et al.* Cross-validation and predictive value of near-infrared spectroscopy algorithms for day-5 blastocyst transfer. *Reprod. Biomed. Online* **22**, 477–484 (2011).
28. Hardarson, T. *et al.* Non-invasive metabolomic profiling of Day 2 and 5 embryo culture medium: A prospective randomized trial. *Hum. Reprod.* **27**, 89–96 (2012).
29. Sfontouris, I. *et al.* Non-invasive metabolomic analysis using a commercial NIR instrument for embryo selection. *J. Hum. Reprod. Sci.* **6**, 133 (2013).
30. Seli, E. *et al.* Noninvasive metabolomic profiling as an adjunct to morphology for noninvasive embryo assessment in women undergoing single embryo transfer. *Fertil. Steril.* (2010). doi:10.1016/j.fertnstert.2009.03.078
31. Vergouw, C. G. *et al.* Day 3 embryo selection by metabolomic profiling of culture medium with near-infrared spectroscopy as an adjunct to morphology: A randomized controlled trial. *Hum. Reprod.* **27**, 2304–2311 (2012).
32. Vergouw, C. G. *et al.* Metabolomic profiling by near-infrared spectroscopy as a tool to assess embryo viability: a novel, non-invasive method for embryo selection. *Hum. Reprod.* **23**, 1499–1504 (2008).
33. Sakkas, D., Botros, L., Henson, M., Judge, K. & Roos, P. Metabolomics: The ViaMetrics-E ™ Procedure for Assessing Embryo Viability. in *Practical Manual of In Vitro Fertilization* 405–412 (2012). doi:10.1007/978-1-4419-1780-5
34. Brison, D. R., Hollywood, K., Arnesen, R. & Goodacre, R. Predicting human

embryo viability: The road to non-invasive analysis of the secretome using metabolic footprinting. *Reprod. Biomed. Online* **15**, 296–302 (2007).
35. Grunert, T., Stephan, R., Ehling-Schulz, M. & Johler, S. Fourier Transform Infrared Spectroscopy enables rapid differentiation of fresh and frozen/thawed chicken. *Food Control* **60**, 361–364 (2016).
36. Rodriguez-Saona, L. E., Giusti, M. M. & Shotts, M. Advances in infrared spectroscopy for food authenticity testing. in *Advances in food authenticity testing* 71–116 (2016). doi:10.1016/B978-0-08-100220-9.00004-7
37. Kosa, G. *et al.* Assessment of the scalability of a microtiter plate system for screening of oleaginous microorganisms. *Appl. Microbiol. Biotechnol.* **102**, 4915–4925 (2018).
38. Sellick, C. A. *et al.* Rapid monitoring of recombinant antibody production by mammalian cell cultures using Fourier transform infrared spectroscopy and chemometrics. *Biotechnol. Bioeng.* **106**, 432–442 (2010).
39. Musmann, C., Joeris, K., Markert, S., Solle, D. & Scheper, T. Spectroscopic methods and their applicability for high-throughput characterization of mammalian cell cultures in automated cell culture systems. *Eng. Life Sci.* **16**, 405–416 (2016).
40. Scholz, T., Lopes, V. V. & Calado, C. R. C. High-throughput analysis of the plasmid bioproduction process in Escherichia coli by FTIR spectroscopy. *Biotechnol. Bioeng.* **109**, 2279–2285 (2012).
41. Bağcıoğlu, M., Fricker, M., Johler, S. & Ehling-Schulz, M. Detection and identification of bacillus cereus, bacillus cytotoxicus, bacillus thuringiensis, bacillus mycoides and bacillus weihenstephanensis via machine learning based FTIR spectroscopy. *Front. Microbiol.* **10**, 1–10 (2019).
42. Vogt, S. *et al.* Fourier-Transform Infrared (FTIR) Spectroscopy for Typing of Clinical Enterobacter cloacae Complex Isolates. *Front. Microbiol.* **10**, 1–11 (2019).
43. Depciuch, J. *et al.* FTIR Spectroscopy of Cerebrospinal Fluid Reveals Variations in the Lipid: Protein Ratio at Different Stages of Alzheimer's Disease. *J. Alzheimer's Dis.* **68**, 281–293 (2019).
44. Blat, A. *et al.* Fourier transform infrared spectroscopic signature of blood plasma in the progression of breast cancer with simultaneous metastasis to lungs. *J. Biophotonics* **12**, 1–11 (2019).
45. Untereiner, V. *et al.* Bile analysis using high-throughput FTIR spectroscopy for the diagnosis of malignant biliary strictures: A pilot study in 57 patients. *J. Biophotonics* **7**, 241–253 (2014).
46. Wenning, M. & Scherer, S. Identification of microorganisms by FTIR spectroscopy: perspectives and limitations of the method. *Appl. Microbiol. Biotechnol.* **97**, 7111–7120 (2013).
47. Ollesch, J. *et al.* It's in your blood: Spectral biomarker candidates for urinary bladder cancer from automated FTIR spectroscopy. *J. Biophotonics* **7**, 210–221 (2014).
48. Zhang, X. *et al.* Profiling serologic biomarkers in cirrhotic patients via high-throughput Fourier transform infrared spectroscopy: Toward a new diagnostic tool of hepatocellular carcinoma. *Transl. Res.* **162**, 279–286 (2013).
49. Peuchant, E. *et al.* Infrared spectroscopy: a reagent-free method to distinguish Alzheimer's disease patients from normal-aging subjects. *Transl. Res.* **152**, 103–112 (2008).
50. Lacombe, C. *et al.* Rapid screening of classic galactosemia patients: A proof-

of-concept study using high-throughput FTIR analysis of plasma. *Analyst* **140**, 2280–2286 (2015).
51. Scott, D. A. *et al.* Diabetes-related molecular signatures in infrared spectra of human saliva. *Diabetol. Metab. Syndr.* **2**, 48 (2010).
52. Bosch, A. *et al.* Fourier transform infrared spectroscopy for rapid identification of nonfermenting gram-negative bacteria isolated from sputum samples from cystic fibrosis patients. *J. Clin. Microbiol.* **46**, 2535–2546 (2008).
53. Lasch, P. *et al.* Antemortem Identification of Bovine Spongiform Encephalopathy from Serum Using Infrared Spectroscopy. *Anal. Chem.* **56**, 6673–6678 (2002).
54. Fabian, H., Lasch, P. & Naumann, D. Analysis of biofluids in aqueous environment based on mid-infrared spectroscopy. *J. Biomed. Opt.* **10**, 031103 (2005).
55. Kosa, G., Shapaval, V., Kohler, A. & Zimmermann, B. FTIR spectroscopy as a unified method for simultaneous analysis of intra- and extracellular metabolites in high-throughput screening of microbial bioprocesses. *Microb. Cell Fact.* **16**, 1–11 (2017).
56. Baker, M. J. *et al.* Developing and Understanding Biofluid Vibrational Spectroscopy: A Critical Review. *Chem. Soc. Rev.* **45**, 1803–1818 (2016).
57. Baker, M. J. *et al.* Clinical applications of infrared and Raman spectroscopy: State of play and future challenges. *Analyst* **143**, 1735–1757 (2018).
58. Lasch, P. & Naumann, D. *Infrared Spectroscopy in Microbiology*. *Encyclopedia of Analytical Chemistry* (2015). doi:10.1002/9780470027318.a0117.pub2
59. Petibois, C., Melin, A. M., Perromat, A., Cazorla, G. & Déléris, G. Glucose and lactate concentration determination on single microsamples by Fourier-transform infrared spectroscopy. *J. Lab. Clin. Med.* **135**, 210–215 (2000).
60. Hackett, M. J. *et al.* Concurrent glycogen and lactate imaging with FTIR spectroscopy to spatially localize metabolic parameters of the glial response following brain ischemia. *Anal. Chem.* **88**, 10949–10956 (2016).
61. Kohler, A. *et al.* High-throughput biochemical fingerprinting of Saccharomyces cerevisiae by Fourier transform infrared spectroscopy. *PLoS One* **10**, 1–22 (2015).
62. Wold, S. & Sjöström, M. SIMCA: A Method for Analyzing Chemical Data in Terms of Similarity and Analogy. in 243–282 (1977). doi:10.1021/bk-1977-0052.ch012
63. Gardner, D. K., Wela, P. & Wale, P. L. Analysis of metabolism to select viable human embryos for transfer. *Fertil. Steril.* **99**, 1062–1072 (2013).
64. Dubey, P. K., Tripathi, A. & Ali, A. Assisted Reproductive Technologies in Infertility Treatment: Opportunities and Challenges. in *Male Infertility: Understanding, Causes and Treatment* (eds. Singh, R. & Singh, K.) 481–497 (Springer Singapore, 2017). doi:10.1007/978-981-10-4017-7
65. Vahlsing, T., Delbeck, S., Leonhardt, S. & Heise, H. M. Noninvasive Monitoring of Blood Glucose Using Color-Coded Photoplethysmographic Images of the Illuminated Fingertip Within the Visible and Near-Infrared Range: Opportunities and Questions. *J. Diabetes Sci. Technol.* **12**, 1169–1177 (2018).
66. Zhang, S. *et al.* Nondestructive Measurement of Hemoglobin in Blood Bags Based on Multi-Pathlength VIS-NIR Spectroscopy. *Sci. Rep.* **8**, 1–9 (2018).
67. Sakudo, A. Near-infrared spectroscopy for medical applications: Current status

and future perspectives. *Clin. Chim. Acta* **455**, 181–188 (2016).
68. Seli, E., Robert, C. & Sirard, M. A. Omics in assisted reproduction: Possibilities and pitfalls. *Mol. Hum. Reprod.* **16**, 513–530 (2010).
69. Bosch, A. *et al.* Rapid discrimination of lactobacilli isolated from kefir grains by FT-IR spectroscopy. *Int. J. Food Microbiol.* **111**, 280–287 (2006).
70. Elder, K. & Dale, B. *In-Vitro Fertilization*. (Cambridge University Press, 2019). doi:10.1017/9781108611633
71. Velde T. & Pearson P. L. The variability of female reproductive aging. *Hum. Reprod. Update* **8**, 141–154 (2002).
72. Albertini, D. F. *et al.* A prognosis-based approach to infertility: understanding the role of time. *Hum. Reprod.* **32**, 1556–1559 (2017).
73. Van Kooij, R. J., Looman, C. W. N., Habbema, J. D. F., Dorland, M. & Te Velde, E. R. Age-dependent decrease in embryo implantation rate after in vitro fertilization. *Fertil. Steril.* **66**, 769–775 (1996).
74. Chuang, C.-C. *et al.* Age is a better predictor of pregnancy potential than basal follicle-stimulating hormone levels in women undergoing in vitro fertilization. *Fertil. Steril.* **79**, 63–68 (2003).
75. Sharif, K., Elgendy, M., Lashen, H. & Afnan, M. Age and basal follicle stimulating hormone as predictors of in vitro fertilisation outcome. *BJOG An Int. J. Obstet. Gynaecol.* **105**, 107–112 (1998).
76. Padilla, S. L. & Garcia, J. E. Effect of maternal age and number of in vitro fertilization procedures on pregnancy outcome. *Fertil. Steril.* **52**, 270–273 (1989).
77. Van Voorhis, B. J. In Vitro Fertilization. *N. Engl. J. Med.* **356**, 379–386 (2007).
78. Hart, R. J. Physiological Aspects of Female Fertility: Role of the Environment, Modern Lifestyle, and Genetics. *Physiol. Rev.* **96**, 873–909 (2016).
79. Palermo, G., Joris, H., Devroey, P. & Van Steirteghem, A. C. Pregnancies after intracytoplasmic injection of single spermatozoon into an oocyte. *Lancet* **340**, 17–18 (1992).
80. Van Steirteghem, A. C. *et al.* High fertilization and implantation rates after intracytoplasmic sperm injection. *Hum. Reprod.* **8**, 1061–1066 (1993).
81. Penzias, A. *et al.* Performing the embryo transfer: a guideline. *Fertil. Steril.* **107**, 882–896 (2017).
82. Lasch, P. Spectral pre-processing for biomedical vibrational spectroscopy and microspectroscopic imaging. *Chemom. Intell. Lab. Syst.* **117**, 100–114 (2012).
83. Helm, D. & Naumann, D. Identification of some bacterial cell components by FT-IR spectroscopy. *FEMS Microbiol. Lett.* **126**, 75–79 (1995).
84. Rebuffo-Scheer, C. A., Dietrich, J., Wenning, M. & Scherer, S. Identification of five Listeria species based on infrared spectra (FTIR) using macrosamples is superior to a microsample approach. *Anal. Bioanal. Chem.* **390**, 1629–1635 (2008).
85. Helm, D. *et al.* Classification and identification of bacteria by Fourier-transform infrared spectroscopy. *J. Gen. Microbiol.* **137**, 69–79 (1991).
86. Zontov, Y. V., Rodionova, O. Y., Kucheryavskiy, S. V. & Pomerantsev, A. L. DD-SIMCA – A MATLAB GUI tool for data driven SIMCA approach. *Chemom. Intell. Lab. Syst.* **167**, 23–28 (2017).
87. Cavelaars, M. *et al.* OpenClinica. *J. Clin. Bioinforma.* **5**, S2 (2015).

ACKNOWLEDGEMENTS

This research was supported by a Merck Serono award, "Grant for Fertility Innovation" GFI-2012-1; by an award from Comisión de Investigaciones Científicas de la Provincia de Buenos Aires, (CIC-PBA), “PREMIO CIENCIA Y COMUNIDAD 2013”; by an award from Ministerio de Ciencia, Tecnología e Innovación Productiva (MINCyT), “PREMIO INNOVAR 2015”; and from a grant of the Fondo para la Investigación Científica y Tecnológica (FONCYT), ANR-800-183/11. C.B.F. was supported by CONICET, Argentina; A.B was supported by CIC PBA. Dr. Donald F. Haggerty, a retired academic career investigator and native English speaker, edited the final version of the manuscript.

AUTHOR CONTRIBUTIONS

C.B.F., M.G., C.B., P.L., J.S., A.K., V.T., V.S., and A.B designed the experiments, supervised research, and wrote and edited the paper. O.M.Y., M.H. and A.B. supervised the project. F.A. and L.G. organized and oversaw the clinical data collection. M.G.P. and C.B. collected embryo culture supernatants and oversaw the sample collection. A.K., V.S., V. T., C.B.F., and A.B. devised and implemented the mathematical models and statistical analyses. All the authors discussed the results and implications.

COMPETING INTERESTS

The authors declare no competing interests.

Correspondence and requests for materials should be addressed to A.B.

FIGURES AND FIGURES LEGENDS

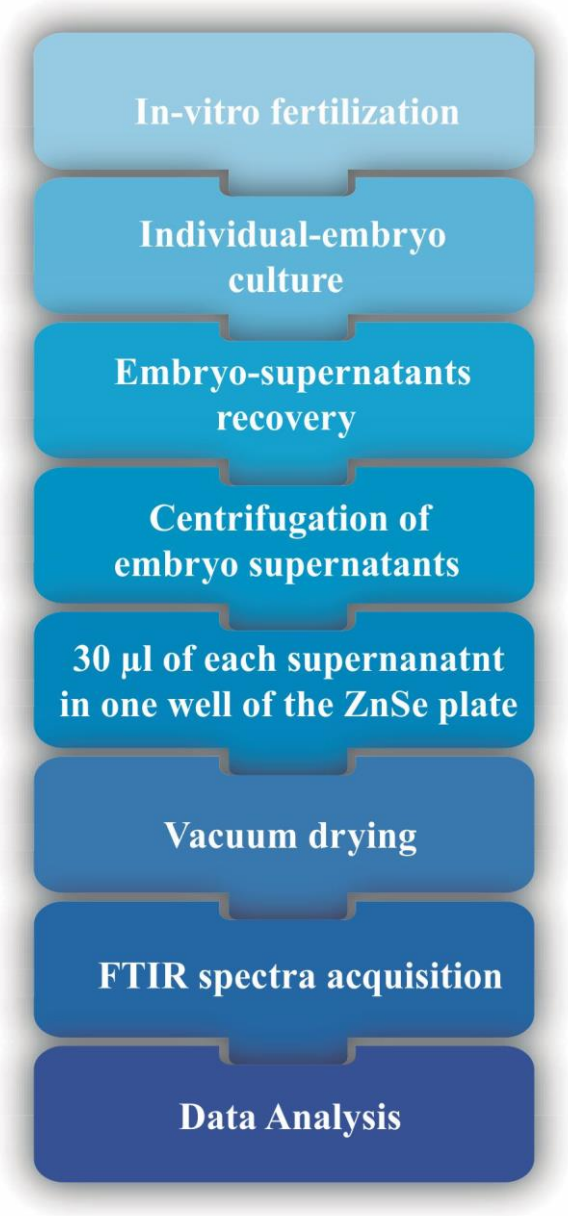

Fig. 1. Flow sheet of the standardized approach for FTIR spectral measurements of embryo supernatant

a

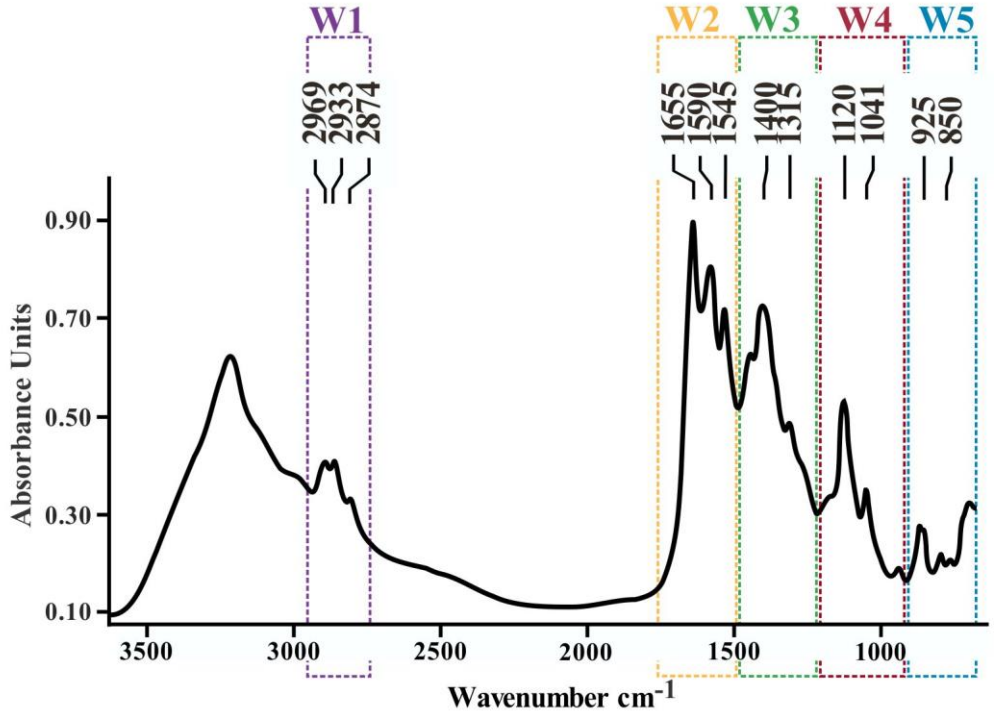

b

Spectral windows (cm-1)		Wavenumber (cm-1)	Band assignment[1]
W1 2800-3000	Aliphatic chains	2969 2933 2874	υ*as* CH_3 υ*as* CH_2 υ*s* CH_3
W2 1500-1800	Proteins and Peptides	1655 1590 1545	υ >C=O and δ C-N δ N-H δ N-H and υ C-N
W3 1200-1500	Mixed region	1400 1,315	υ -COO υ C-N and δ N-H
W4 900-1200	Carbohydrate	1120 1041	υ C-O
W5 650-900	Fingerprint region	925 850	υ O-H out of plane υ*s* C-O-C

Fig. 2. Spectral description of embryo-culture supernatants. Panel a: FTIR spectrum of a 3-day-embryo supernatant recovered from the culture of an embryo of class IMP. The main spectral windows (W1 to W5) indicated above the figure correspond to: W1 aliphatic chains, (2800–3000 cm^{-1}), W2 the region assigned to protein absorptions (1500–1800 cm^{-1}), W3 the mixed region (1200–1500 cm^{-1}), W4

931 the region assigned to carbohydrate-absorption bands (900–1200 cm^{-1}), and W5 the
932 fingerprint region (650–900 cm^{-1}). υ = stretching vibrations, *s* = symmetric
933 vibrations, and *as* = antisymmetric vibrations, δ = bending. Panel b: Spectral
934 windows associated with functional groups in biomolecules and the band assignments
935 for the 3-day-embryo supernatants.
936

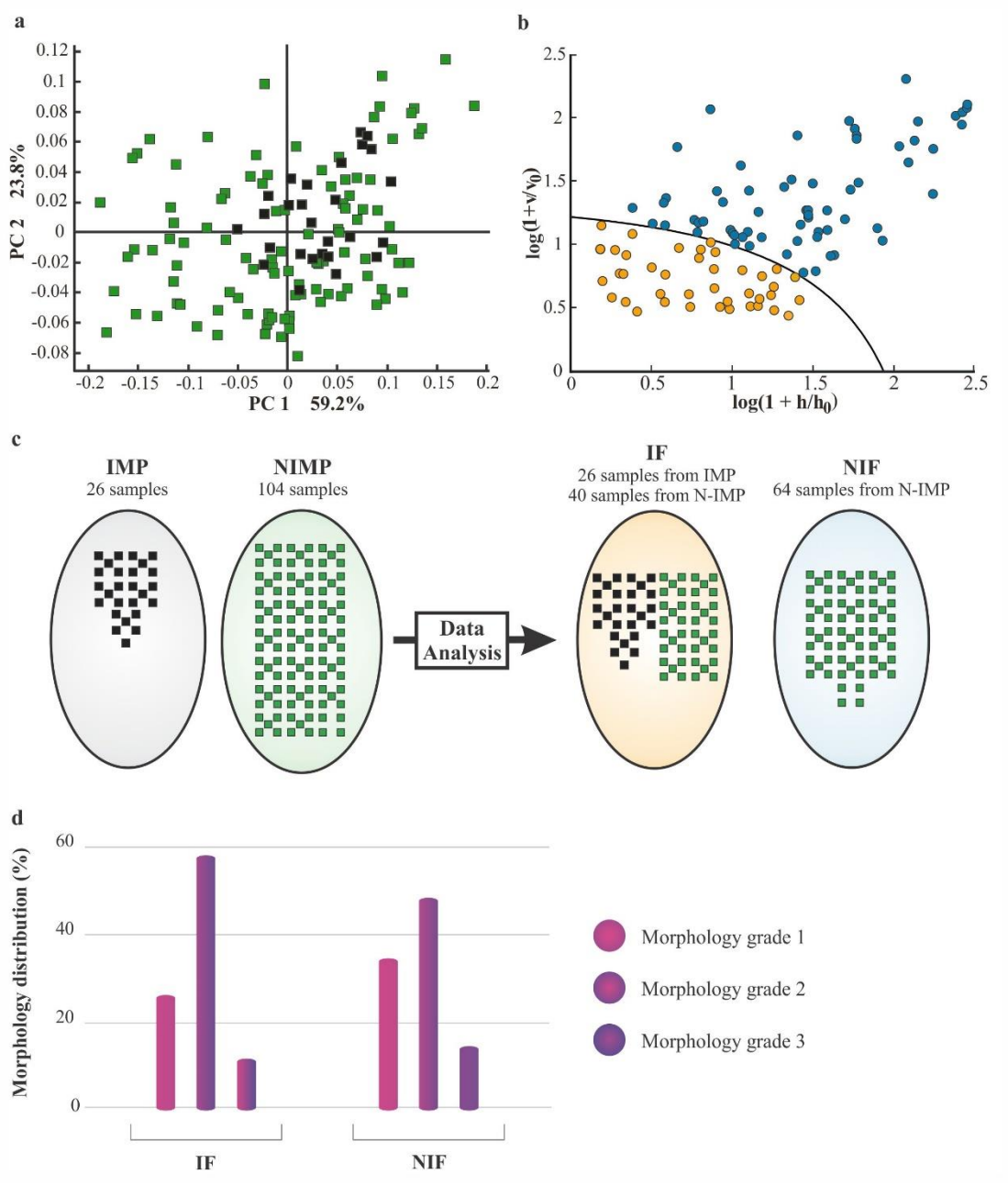

937

Fig. 3. Metabolomics study of embryos based on FTIR spectroscopy in combination with multivariate analyses. Panel a: PCA-score plot based on FTIR metabolic fingerprinting of embryo-culture supernatants. Black squares, class IMP, (spectra of supernatants from embryos that implanted at 100%); green squares, class NIMP (spectra of supernatants for embryos that did not implant at 0% implantation). Panel b: Classification of the results for class-NIMP data by SIMCA modelling. Orange dots, class IF (implantation fingerprinting); blue dots, class NIF (nonimplantation fingerprinting). Panel c: Logic diagram indicating the distribution of samples according to the implantation outcomes (IMP *versus* NIMP) and their assignment to the IF or NIF groups according to the results obtained by the PCA and SIMCA analyses. The IF group comprises all the IMP spectra (26 samples) and a fraction of the NIMP spectra with features of the metabolic implantation fingerprint (40 samples), while the NIF group contains nonimplantation fingerprints from the NIMP spectra (64 samples). Panel d: Distribution of embryo-morphology qualities as determined by the Istanbul consensus within the IF and NIF groups (morphology grade 1, morphology grade 2, morphology grade 3). The percent distribution of the different morphological grades is plotted on the *ordinate* for the two metabolomic classes indicated on the *abscissa*. The statistical analysis revealed no significant differences between the embryo-morphology grades observed with the IF and the NIF patterns ($p = 0.125$).

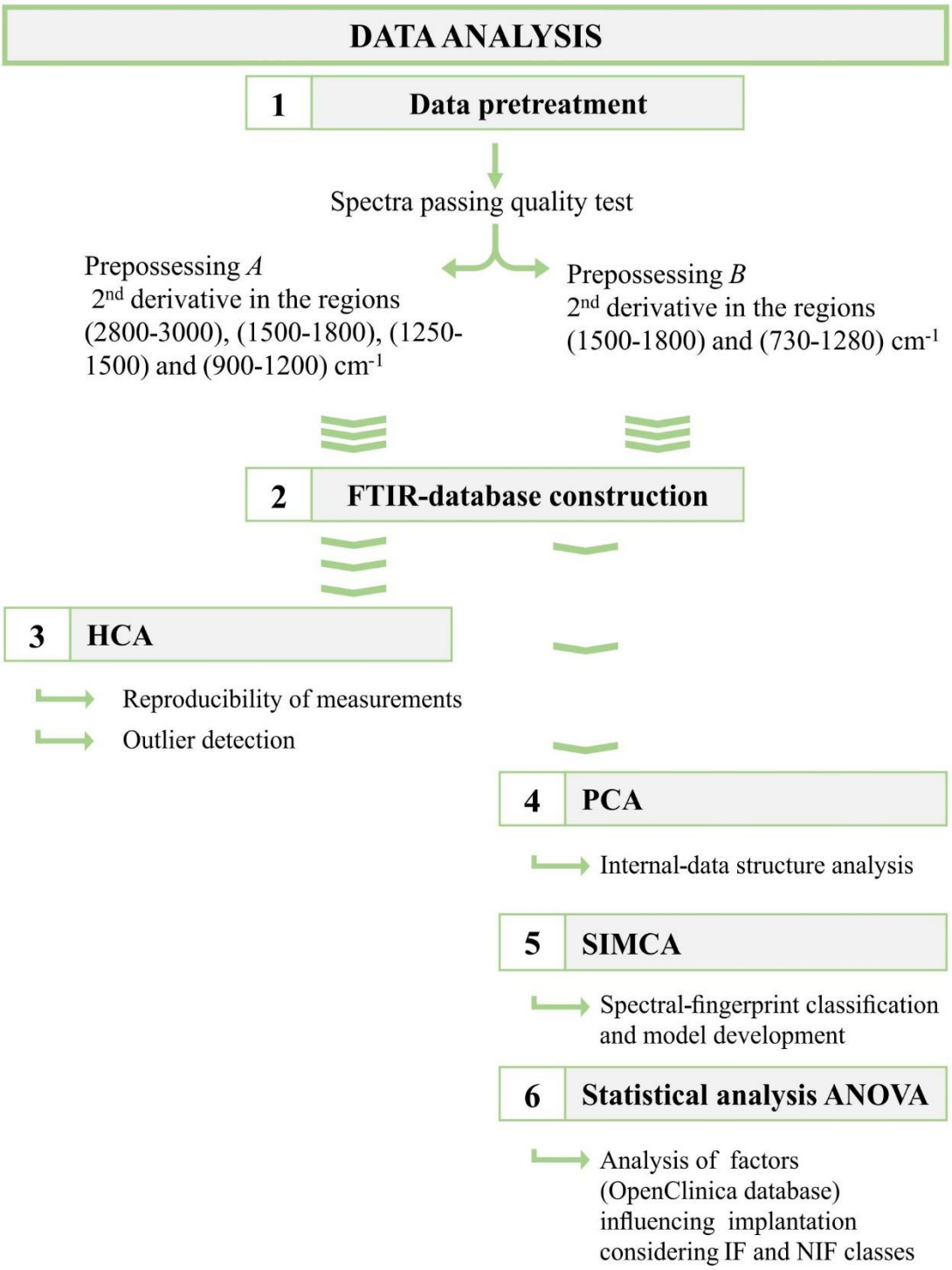

959

960 **Fig. 4. FTIR-spectral–data-analysis flow chart for embryo supernatants.**

961

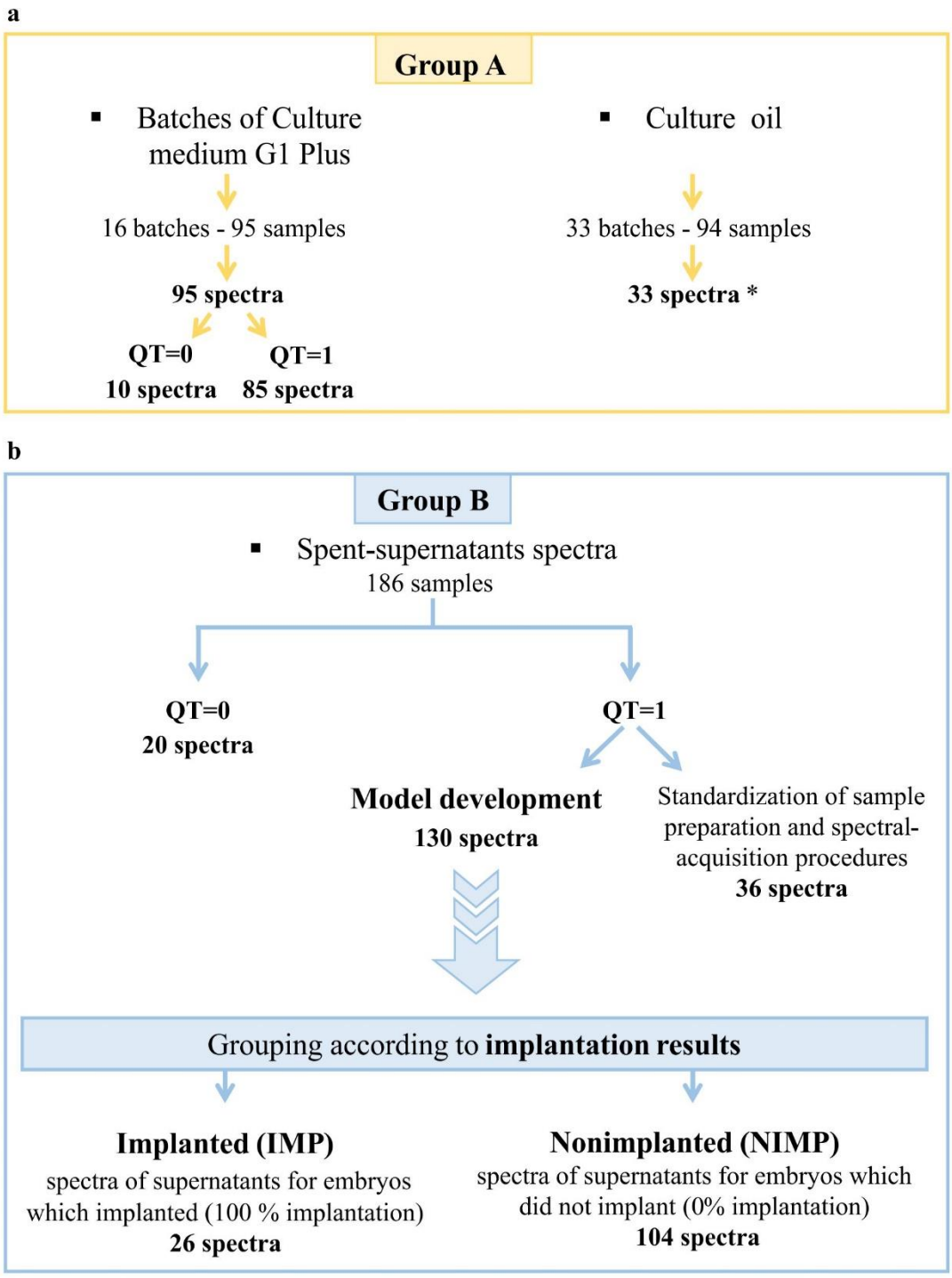

962

963 **Fig. 5. FTIR spectral database construction.** Panel a: Scheme illustrating the details
964 of the control samples (Group A) analyzed by FTIR spectroscopy from the embryo-
965 culture media along with the results from quality-testing (QT) criteria, and from the
966 culture oil used. Panel b: Scheme depicting the details of the samples analyzed for
967 FTIR spectroscopy from the spent supernatant media from cultures of embryos that

were transferred to patients, indicating the embryos that implanted and those that failed to do so along with the quality-testing results of the corresponding sample groups (Group B). The bottom window of Panel b summarizes the spectra of the supernatants associated with the different outcomes of the embryo transfers for implantation, indicated by implantation (IMP) and nonimplantation (NIMP) QT = 1, fulfilled the spectral-quality requirements, QT = 0 did not meet the spectral-quality requirements.

*Only one sample from each batch was measured.

Figures

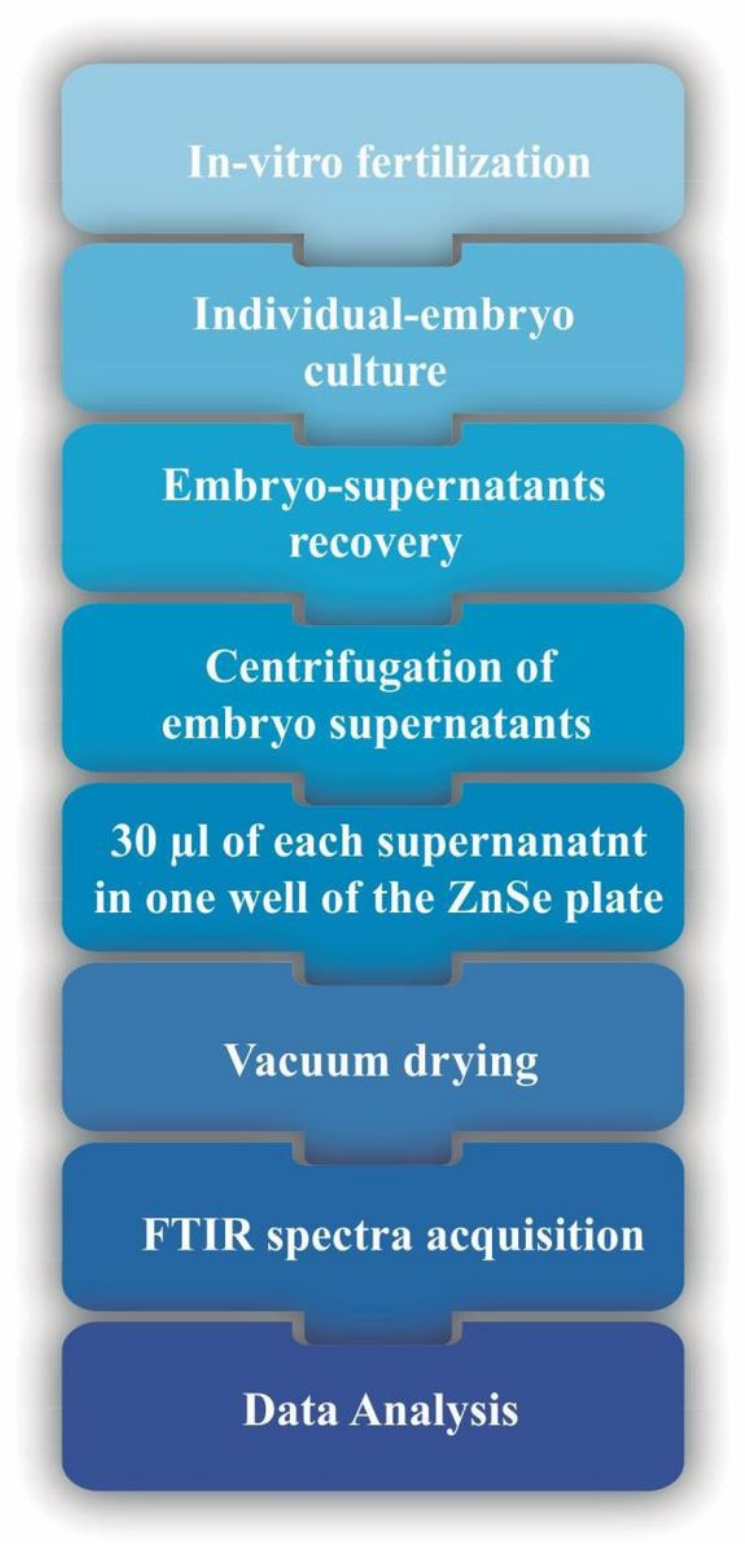

Figure 1

Flow sheet of the standardized approach for FTIR spectral measurements of embryo supernatant

a

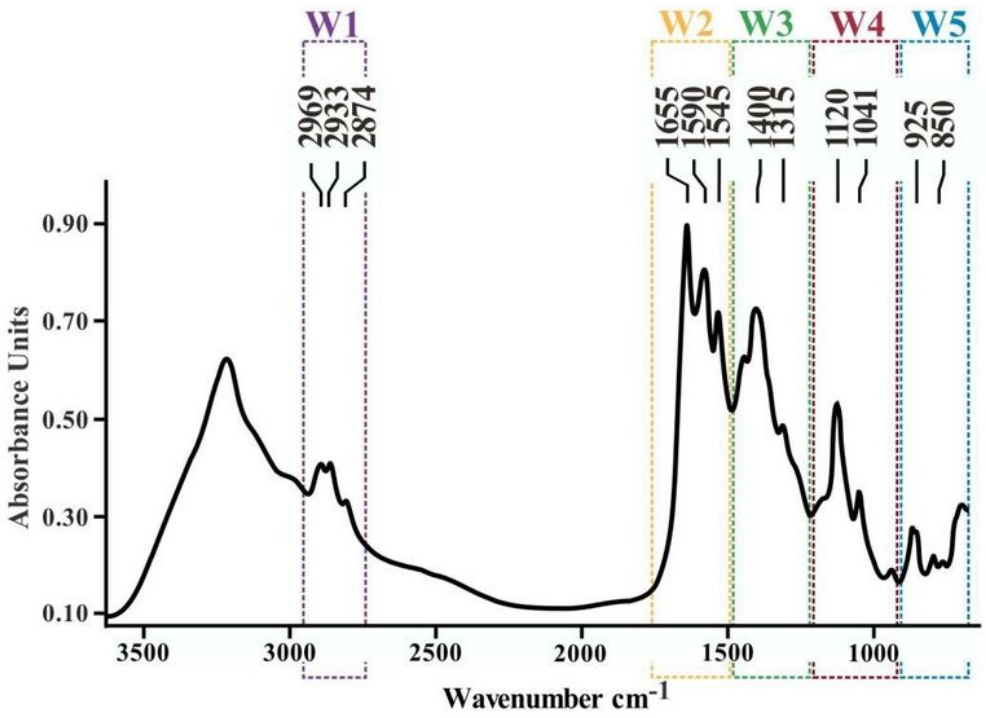

b

Spectral windows (cm-1)		Wavenumber (cm-1)	Band assignment[1]
W1 2800-3000	Aliphatic chains	2969 2933 2874	υ*as* CH_3 υ*as* CH_2 υ*s* CH_3
W2 1500-1800	Proteins and Peptides	1655 1590 1545	υ >C=O and δ C-N δ N-H δ N-H and υ C-N
W3 1200-1500	Mixed region	1400 1,315	υ -COO υ C-N and δ N-H
W4 900-1200	Carbohydrate	1120 1041	υ C-O
W5 650-900	Fingerprint region	925 850	υ O-H out of plane υ*s* C-O-C

Figure 2

Spectral description of embryo-culture supernatants. Panel a: FTIR 926 spectrum of a 3-day-embryo supernatant recovered from the culture of an embryo of 927 class IMP. The main spectral windows (W1 to W5) indicated above the figure 928 correspond to: W1 aliphatic chains, (2800–3000 cm–1), W2 the region assigned to 929 protein absorptions (1500–1800 cm–1), W3 the mixed region (1200–1500 cm–1), W4 the region assigned to carbohydrate-absorption bands (900–1200 cm–1), and W5 the 931

fingerprint region (650–900 cm–1). v= stretching vibrations, s = symmetric 932 vibrations, and as = antisymmetric vibrations, u = bending. Panel b: Spectral 933 windows associated with functional groups in biomolecules and the band assignments 934 for the 3-day-embryo supernatants.

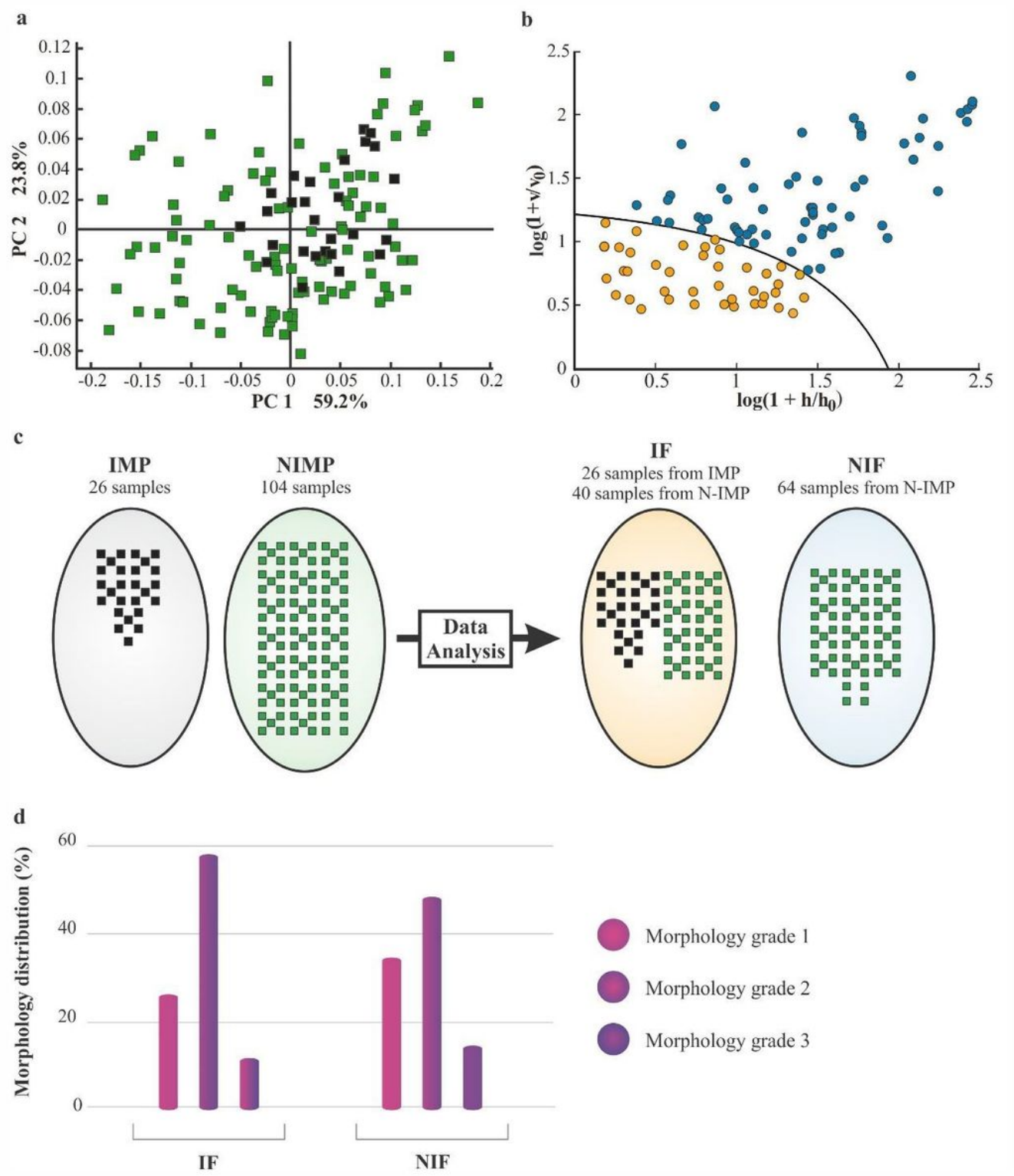

Figure 3

Metabolomics study of embryos based on FTIR spectroscopy in combination with multivariate analyses. Panel a: PCA-score plot based on FTIR metabolic fingerprinting of embryo-culture supernatants. Black

squares, class IMP, (spectra of supernatants from embryos that implanted at 100%); green squares, class NIMP (spectra of supernatants for embryos that did not implant at 0% implantation). Panel b: Classification of the results for class-NIMP data by SIMCA modelling. Orange dots, class IF (implantation fingerprinting); blue dots, class NIF (nonimplantation fingerprinting). Panel c: Logic diagram indicating the distribution of samples according to the implantation outcomes (IMP versus NIMP) and their assignment to the IF or NIF groups according to the results obtained by the PCA and SIMCA analyses. The IF group comprises all the IMP spectra (26 samples) and a fraction of the NIMP spectra with features of the metabolic implantation fingerprint (40 samples), while the NIF group contains nonimplantation fingerprints from the NIMP spectra (64 samples). Panel d: Distribution of embryo-morphology qualities as determined by the Istanbul consensus within the IF and NIF groups (morphology grade 1, morphology grade 2, morphology grade 3). The percent distribution of the different morphological grades is plotted on the ordinate for the two metabolomic classes indicated on the abscissa. The statistical analysis revealed no significant differences between the embryo-morphology grades observed with the IF and the NIF patterns ($p = 0.125$).

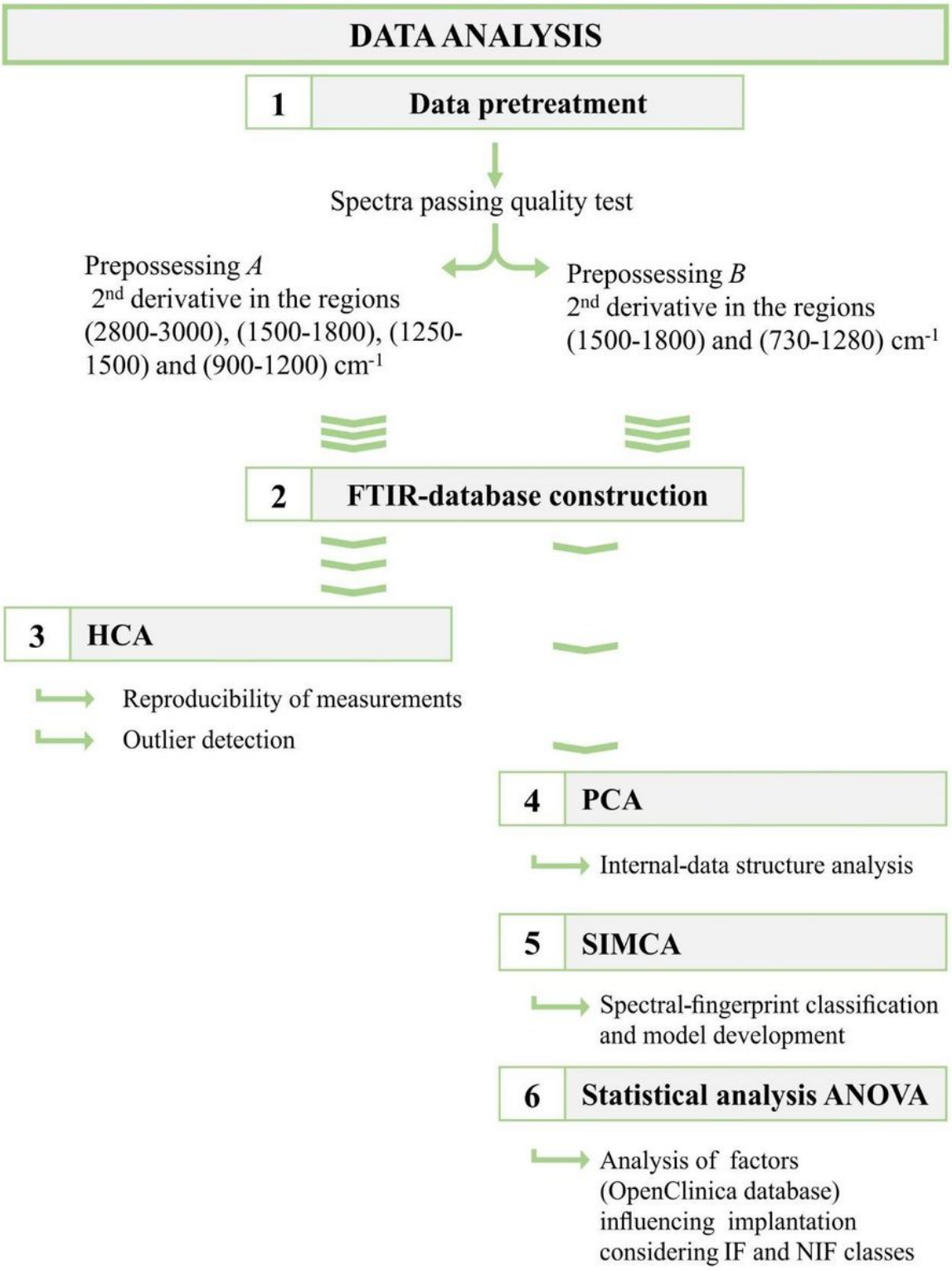

Figure 4

FTIR-spectral–data-analysis flow chart for embryo supernatants.

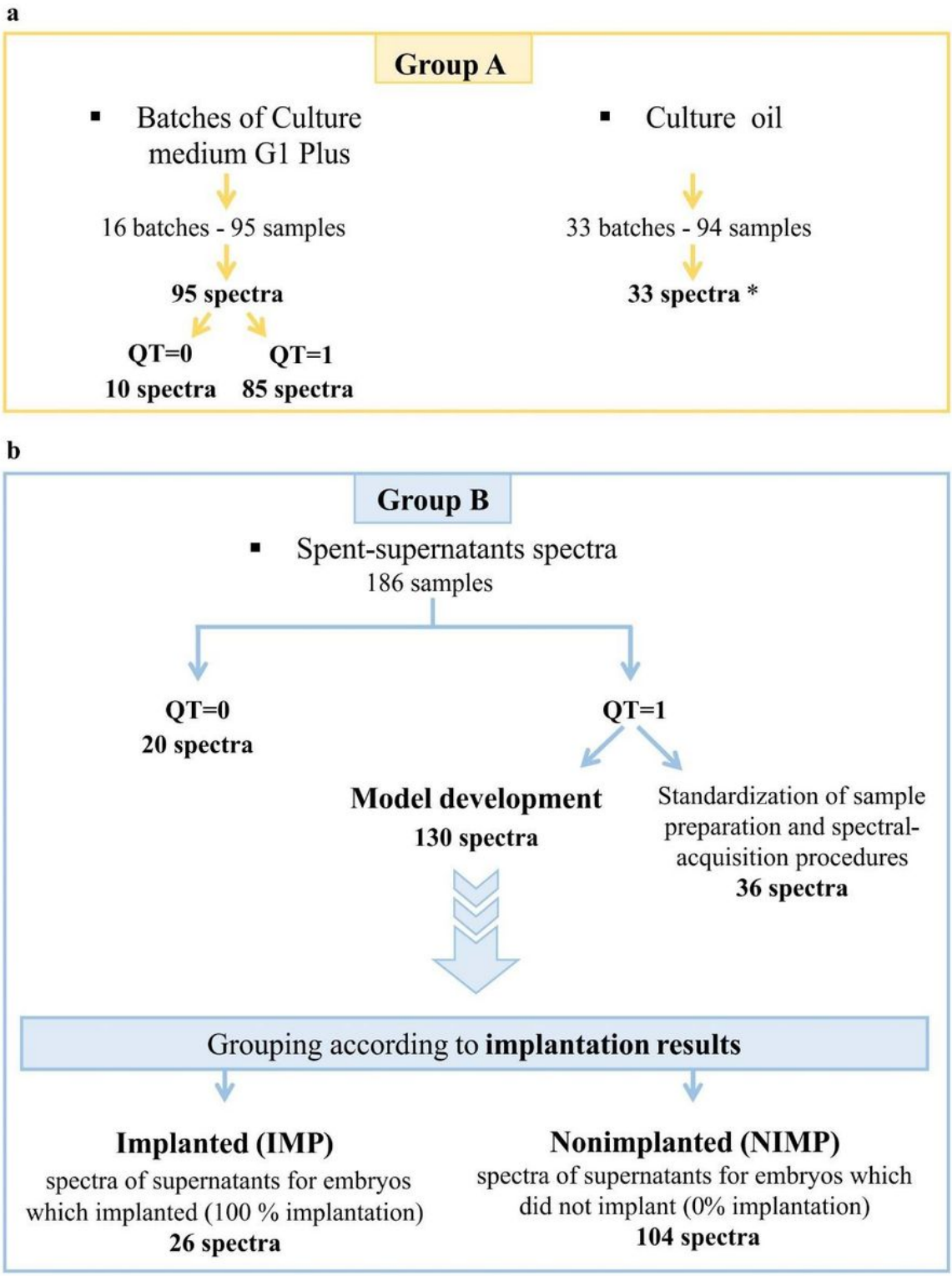

Figure 5

FTIR spectral database construction. Panel a: Scheme illustrating the details of the control samples (Group A) analyzed by FTIR spectroscopy from the embryo- culture media along with the results from quality-testing (QT) criteria, and from the culture oil used. Panel b: Scheme depicting the details of the samples analyzed for 9FTIR spectroscopy from the spent supernatant media from cultures of embryos that were transferred to patients, indicating the embryos that implanted and those that failed to do so

along with the quality-testing results of the corresponding sample groups (Group B). The bottom window of Panel b summarizes the spectra of the supernatants associated with the different outcomes of the embryo transfers for implantation, indicated by implantation (IMP) and nonimplantation (NIMP) QT = 1, 972 fulfilled the spectral-quality requirements, QT = 0 did not meet the spectral-quality requirements. *Only one sample from each batch was measured.

Supplementary Files

This is a list of supplementary files associated with this preprint. Click to download.

- Supplementaryinformation.pdf